Defense Against Chemical Warfare Agents and Toxic Industrial Chemicals (TICS)

Margaret M. Hurley
US Army Research Laboratory (ARL), Aberdeen Proving Ground, MD
hurley@arl.army.mil

Alex Balboa
Edgewood Chemical Biological Center (ECBC), Aberdeen Proving Ground, MD
axbalboa@sbccom.apgea.army.mil

Jeffrey B. Wright
US Army Soldier and Biological Chemical Command (SBCCOM), Natick, MA
Jeffery.Wright@natick.army.mil

Gerald H. Lushington and Jianxin Guo
University of Kansas, Lawrence, KS
{glushington, guo}@ku.edu

1. Introduction

Acetylcholinesterase (AChE) helps to regulate some of the most fundamental human biological operations such as motor function, sleep, attention, memory and emotions. A wide variety of AChE inhibitors exist, with health implications that range from fatal to benign. Strong AChE inhibitors such as some organophosphorus (OP) nerve agents (some of which can phosphorylate AChE irreversibly) are among the most powerful neurotoxins known and pose severe human health risks if misused. Weaker ligands, however, have been broadly studied as possible therapeutics for neural dysfunction disorders such as myasthenia gravis (MG), and various dementia such as Alzheimer's disease (AD). Weaker inhibitors have also been employed for nerve agent prophylaxis, although safety concerns continue to surround the standard prophylaxic formulations, especially pyridostigmine bromide (PB)[1], suggesting that the criteria for their approval for military use might not be acceptable for broader civilian medical application. In fact, demonstrably safe and effective nerve agent prophylaxes remain elusive, despite a wealth of AChE inhibition data arising from AD and MG pharmaceutical research, as well as from pesticide toxicology studies. Prophylaxis design is inherently more challenging than simple inhibitor design, as one must find a balance between an interaction strong enough to prevent adhesion of other ligands but weak enough to permit return to normal enzyme function in a reasonable time frame. These dynamic and competitive factors make prophylaxis difficult to optimize via most standard in vitro assays but lend themselves very well to molecular simulations.

This project uses a variety of modeling techniques to AChE inhibitor kinetics and dynamics to elucidate and evaluate prospective new prophylaxes for nerve agent toxicity threats. Three levels of theory are employed to address the following aspects of this extremely complex problem:

Virtual screening of inhibitor formulation: Multiple AChE inhibitor scaffolds are already known, thus ensuring that sizeable virtual libraries of potential prophylaxes can be constructed using conventional drug design techniques. The computational rigor of prophylaxis evaluation requires extensive prescreening via methods such as Quantitative Structure Activity Relationships (QSARs) and molecular docking. To accomplish this for the challenging AChE binding environment (multiple binding subsites and ligand conformational modes), we have employed three dimensional (3D) QSAR type correlations to formulate a weighted residue-based scoring methodology specifically tailored toward accurately evaluating AChE docking results and formulating de novo inhibitors based on the resulting 3D receptor interaction field.

Analysis of competitive transport kinetics: Fundamental to the high AChE enzymatic efficacy is a collaborative network of receptor subsites that dynamically guide ACh (or inhibitors) toward the esteratic subsite[2]. Comparing the transport properties of different ligands and their competition for access to (and transit past) these subsites will provide insight into the requirements for effective prophylaxis. Such analysis, as well as quantification of transport kinetics, is readily accomplished through MD simulations of prophylaxes and toxins (alone or in competition) interacting with the solvated receptor environment.

Prediction of adsorption kinetics, thermodynamics, and physical properties: Predicting reaction kinetics and thermodynamics of nerve agents and prospective prophylaxes requires the use of QC methods. This data is used to predict bound state geometries and transition states for receptor-ligand complexes, and to

employ the corresponding complex energies to characterize their associated thermodynamics and chemical kinetics. Much time and effort has been expended in delineating the precise interactions within the active site and neighboring residues upon binding. Besides the obvious intrinsic worth of data providing detailed information on the structural features which stabilize binding, unbinding, and related side reactions (such as aging), these results provide an excellent starting point for mutagenesis studies to provide further insite into agent binding. QC studies have also been performed to analyze the gas phase behavior of hydration complexes of nerve agent simulants, as a step toward understanding the ambient volatility of these systems.

2. Computational Details

Virtual Screening of Inhibitor Formulation: The AChE crystal structures used herein were obtained from the PDB database (http://www.rcsb.org). Our main docking and training activities have been focused on a human AChE (huAChE) structure (code#:1B41[3]), but rely on ligand binding information from a torpedo california AChE (tcAChE) structure (code#:1EVE[4]) that includes a co-crystallized E2020 inhibitor. All waters were removed from the structures. The huAChE structure was aligned to the tcAChE in SYBYL[5] to ascertain the orientation of the ligand E2020 relative to the huAChE structure. The Root-Mean Square Derivation (RMSD) between the two is only 0.85 Å for all backbone C_β atoms in those structures, suggesting good alignment and structural similarity. Hydrogen atoms were added (via SYBYL) to the resulting huAChE-E2020 complex. The positions of these new protons were then optimized in MOE[6] via molecular mechanics using the MMFF94s force field (all heavy atoms fixed) to avoid bad inter-atomic contacts. The position of E2020 was then optimized (all receptor atoms fixed) to determine a plausible stable conformational structure for the ligand in the receptor environment. In both of the above simulations, MMFF94s charges were used to account for relevant electrostatics. The Steepest Descent minimization algorithm was used for the first 100 steps (unless a RMS gradient of less than 100 kcal/(mol·Å) was first achieved), followed by 200 steps of Conjugate Gradient (unless a RMS gradient of less than 1 kcal/(mol·Å) was attained), and finally completed by 1000 steps of Truncated Newton (or a RMS gradient of less than 0.01 kcal/(mol·Å)). The resulting E2020 structure was then extracted for subsequent docking calculations.

A collection of 69 compounds with IC50 data measured with human AChE assay[7,8,9] was selected for training and testing the scoring function. The activity among these compounds ranges from 0.33 nM to 30,000 nM. Docking calculations were carried out with the GOLD program[10]. A genetic algorithm was used in searching the binding conformation of flexible ligands, using the default parameters in GOLD. The active site for the huAChE docking calculations was constructed from the crystal structure by retaining all residues within a radius of 12 Å relative to E2020 (but discarding the original ligand itself). A maximum of 20 poses were computed for each compound. Those docked conformations were saved in SDF format and then imported into SYBYL for scoring calculations according to the FlexX and CSCORE modules. The scoring methods available included empirical methods such as Chem score, FlexX score, and G score, and knowledge-based methods such as PMF score and Drug score. Multi-Linear Regression (MLR) was used to obtain a consensus score from these methods. One conformation was selected for each compound, so as to give a good compromise between the best consensus score and those with the closest alignment to the original E2020 ligand. The chosen conformations were used to fit an interaction field of the following form:

$$pIC50 = \sum_i C_i E_i^{ele} + \sum_j d_j E_j^{vdw} \qquad (1)$$

Where c_i, d_j are fitted coefficients, E_i^{ele}, E_j^{vdw} are electrostatic and VDW interactions arising between atoms in the i^{th}, j^{th} residue and the ligand. In this expression, all receptor residues within 10 Å of the position of the original E2020 ligand (a total of 92 residues) were included in the summation over i, and E_i^{ele} and E_j^{vdw} calculated via an SVL script written for the MOE system. The statistic analysis was performed in Simca-P[11] with partial least square regression (PLS). Fifty-three of the full 69 compounds were selected as our training set, and the other 16 compounds were used as a test set for validating the predictive power of the new scoring function.

Competitive Transport Kinetics: In order to arrive at starting structures for simulations of the above collection of ligands interacting with the tcAChE receptor, bond distances and angles for each ligand were optimized via quantum chemical HF/6-31G(d,p) calculations. The resulting structure was then allowed to torsionally relax within the receptor environment and was generated via FlexX molecular docking simulations. In each case, the ligand-receptor complex with the top score (out of 50 docking runs per ligand) as determined by the Drug Score evaluation scheme (along with a visual sanity check) was used as a starting point for further simulations. The ligand—enzyme complex was then protonated via the X-LEaP program distributed within the AMBER 6

software suite[12]. For all calculations, glutamate and aspartate monomérs were modeled in their anionic form, lysines were described as cations, N^{δ} on histidines were protonated, while N^{ε} were left in unprotonated sp^2 hybridized form. All other residues were left in their neutral form, except (for one set of calculations) the deprotonated ser 200 anion. Negative charges were balanced with Na+ ions added according to a coulomb potential on a 1.0 Å grid. In each case, the resulting complex was then fully solvated within an aqueous box defined by a solvent buffer of 7 Å using the TIP3P model. To ensure solvent conservation, three dimensional periodicity was effected via an Ewald summation. RESP atomic charges for the ligand (and the anionic serine residue) were derived from Hartree-Fock/6-31G(p,d) quantum chemical calculations using the antechamber module in amber7.0. Atomic charges for all other enzyme atoms corresponded to the default charges available in the Amber 99 force field. All subsequent classical simulations were effected with the AMBER 6 program, using the Amber 99 force field. The solvated receptor-ligand complex was minimized via standard molecular mechanics for 1000 steps in order to eliminate unrealistic atomic contacts. The system was then equilibrated at constant pressure from 0-300 Kelvin via a 20 ps variable temperature MD simulation with a time step of 2 fs. This relaxed the ligand-receptor complex and its solvent shell, permitting the box to swell to dimensions of slightly less than 80 × 80 × 80 $Å^3$. Equilibration also has the effect of randomizing the ligand conformation and position within the receptor. From this relaxed and randomized structure, dynamic analysis on the system was effected via a 1 ns constant volume simulation in which the system was warmed from 100–300 K. In each case, the entirety of the trajectory, except approximately the first 30 ps of the simulation, persisted within a 295–305 K temperature window that permitted reasonable isothermal analysis.

Prediction of Adsorption Kinetics, Thermodynamics, and Physical Properties: All calculations are performed with the Gaussian suite of codes[13]. Starting structures for acetylcholinesterase are obtained from X-ray crystallographic data and coordinates for the residues of interest are extracted using the RASMOL code. The largest models incorporate the active site residues (Ser200, His440, and Glu327 in the Torpedo Californica numbering), the oxyanion hole residues (Gly118, Gly119, and Ala201), and Glu199. Calculation are performed at the using density functional theory B3LYP (unless otherwise noted) with the 3-21G basis set. These results are then used as the initial structure for optimization, frequency and NMR calculations performed at b3lyp/6–31g(d,p), unless otherwise noted.

3. Results

Virtual Screening of Inhibitor Formulation: Our scoring model built via PLS regression over interactions within the 53 molecule training set appears to be of reasonable quality, with a correlation coefficient of R^2=0.89 and a leave-one-out cross-validation correlation of Q^2=0.72. In using the scoring function to evaluate the activity for the 16 molecules testing set, we achieved good predictivity, a correlation of R^2=0.69 between the calculated results and experimental values.

To compare the precision and extensibility of our scoring function, we contrasted the above results with predictions made using several commercially available scoring methods, including Chemscore, Flex score, Drug score, G score and PMF score. The correlation between the experiment and any single score method is poor. The PMF score showed the best correlation but was still rather poor (R^2=0.13 for the training set). All of the other representations gave even worse correlations: ChemScore = 0.07, FlexX = 0.05, DrugScore = 0.01, G Score = 0.004. Since those general scoring methods were not trained in this AChE inhibition set, it is not completely fair to compare them directly with our specially-tailored energy decomposition method. Therefore, we built a consensus score by training (over the 53 molecule set) a weighted sum over the above five commercially available scoring functions as follows:

$$\text{pIC50} = 0.05682 * \textbf{Chemscore} - 0.00499 * \textbf{Drugscore} - 0.03582 * \textbf{Flexscore} - 0.01232 * \textbf{Gscore} + 0.01847 * \textbf{PMFscore} + 7.62820 \quad (2)$$

where **Chemscore**, **Drugscore**, **Flexscore**, **Gscore** and **PMFscore** refer to computed affinities from the Chem-score, Drug-score, Flex-score, G-score and PMF-score methods respectively. Although an improvement was found for this consensus score within the training set itself (R^2 = 0.26), its predictive potency is poor, judging by no evident correlation within the 16 molecule testing set.

To help verify the physical sensibility of our model, we have mapped out the residues that contribute significantly to the scoring function. Coefficients for the 20 most important residues in terms of electrostatic and VDW contributions are shown in Figure 1. Negative coefficients in this figure can be interpreted as indicating ligand-residue interactions that enhance the binding affinity, while positive coefficients correspond to interactions that diminish the affinity. In terms of absolute magnitude, Trp86, Ile451, Gly448, Tyr449, Ser229 are the most important residues in the active site for VDW interactions. Trp86 enhances ligand binding affinity by forming π-π interaction with ligand aryl groups (when available), while the other residues play a largely steric role by defining the shape of the gorge base, thus serving to discriminate according to ligand shape. In

the upper gorge area, residues Tyr124, Phe295, Phe338, Phe297 are responsible for providing hydrophobic contacts. The ring of Tyr72 is almost perpendicular to the Trp286 ring and forms a blocking wall to prevent the ligand ring moving away from the position forming π-π interaction with the Trp286 ring. Phe295, Phe297, Val365 and Glu292 form another wall on the other side of the PAS.

Residues Tyr449, Glu450, Ile451, Ala127, Ser128, Tyr133, Ile118 near Try86 and the "oxyanion hole" residues Gly121, Gly122 are important in providing electrostatic interactions in the active site. Tyr337, Asp74, Thr83 and Asn87 are the primary electrostatic contributors in the gorge area. Gly342, Lue76, Glu285, Trp286, His287 and Gln291 likely help to enhance the activity of ligands with polar groups oriented in this area, as evidenced by reports that an AChE inhibitor tethering in the position of His287 can affect the binding affinity as much as 14-fold. Site-directed mutagenesis in huAChE indicated that Asp74, Tyr337, Phe338, Phe295, Phe297, Tyr133, Glu450 can affect the affinity although it has been difficult to determine experimentally whether these residues contribute mainly electrostatic or VDW interactions.

The docked ligand structures generally support the above analysis regarding the identity or principle residues. In our current docking calculations, molecules 2–7 all share similar conformations in the PAS. The modified groups in those molecules are actually exposed in the solvent and do not contribute directly to the ligand-receptor interaction. This is the same as observed in previous studies[8]. However, in the current work, molecule 8 takes a slightly different conformation with its morpholino group situating in the half-buried packet by Trp286, His287, Ser293, Glu292 and Leu289. The morpholino Oxygen has a distance of 3.65 Å to the backbone N of Glu292, and the morpholino Nitrogen is 3.78 Å from the backbone O of Ser293. Such interactions could slightly pull the benzisoxazole ring away from Trp286 ring, leaving only a partial π-π interaction. This particular conformation leads to an affinity increased by more than 10-folds to 0.8nM relative to molecules 2–7. This particular region has been confirmed in an x-ray structure to be very important for the inhibitors binding to the PAS (periferal anionic site).

As a final point of validation, we compared the calculated conformation for E2020 within the huAChE crystal structure relative to its original co-crystallized conformation in tcAChE. Our calculated structure suggests that E2020 has similar but not identical binding modes in tcAChE and huAChE. In the active site, its benzyl ring forms a π-π interaction with the indole ring of Trp86 in huAChE and Trp84 in tcAChE. In the PAS, the indanone ring of E2020 forms a π-π interaction with the indole ring of Trp286 in huAChE and Trp279 in tcAChE. The charged nitrogen of the E2020 piperidine ring undergoes a cation-π interaction with the phenyl ring of Phe330 in tcAChE. The corresponding residue Tyr337 in huAChE does not form a similar cation-π interaction due to the steric limitations in this area associated with an inauspicious orientation of the Tyr337 ring. As a result, the nitrogen of the piperidine ring of the E2020 instead interacts with the hydroxyl groups of the Tyr337, Tyr124 and Ser125 within distances of 3.41, 3.12 and 4.18 Å relative to the oxygen atom of the respective hydroxyl groups. To probe the role of Tyr337, we examined the potential energy curve for Tyr337 side chain rotation relative to the other residues (energy evaluation according to the MMFF94s force field with appropriate charges), but found there to be only one minimum in the potential curve. Closer analysis reveals that that the Tyr337 ring is trapped in a local pocket formed by Phe338, Tyr341, Trp439, Trp449 and His447. In previous structural studies and molecular dynamics simulations, it has been found that Phe330 in tcAChE can adopt a wide range of conformations in the complex structure and may function as a swinging gate that structurally couples the anion sub-site of the active site and the PAS. It is natural to expect similar behavior of Tyr337 in the huAChE as compared with the analogous Phe330 in tcAChE. Such a gate swing movement of the Tyr337 ring would certainly induce a shift in attached and neighboring residues, thus one function of this PAS/active site coupling could be to effect proper residue alignment within the anionic subsite. The fact that the huAChE crystal structure used in this study to train our scoring function did not have a co-crystallized active site inhibitor (having only a PAS-bound fasciculin molecule) and thus did not reflect such a conformational shift in the Tyr337 may constitute a subtle flaw in our model. Given our model's fairly strong predictive capacity, we expect the flaw to be of only minor consequence, however.

Competitive Transport Kinetics: The Torpedo Californica AChE receptor cavity entails one hydrophobic end demarcated by Trp 84, and a polar side including His 440 and Ser 200 that initiates the hydrolysis reaction. Molecules such as ACh and many of the OP nerve agents have both hydrophobic and polar groups, thus one can envision a possible binding mechanism such that the hydrophobic end of the ligand is attracted to the gorge region by the lipophilic periferal site, migrates to the deeper Trp 84 residue, and then swings its polar electrophilic group down toward Ser 200. The tendency toward such behavior can be measured in MD simulations by tracking center of mass movements throughout the trajectory. The progression of a soman molecule has been monitored throughout the 1 ns simulation (Ser 200 treated anionically). This initial exterior starting position leads to rapid (~30 ps) admission into the gorge, at which point its hydrophobic 1,2-dimethyl-propyl group remains fairly

well coupled to Trp 84. A similar simulation of DFP yielded almost identical behavior, strongly suggesting that relatively small molecules such as ACh and most OP nerve agents are drawn rapidly into the cavity.

Once in the cavity, however, little evidence is found for strong coupling between the ligand's polar phosphonate group and Ser 200. This is indeed case for all of the simulations undertaken with the deprotonated Ser 200. This is further reflected in studying the distances (R_{CO}) beween the ester carboxyl carbon of ACh and the side chain oxygen of Ser 200. The R_{CO} arising from the trajectory are summarized according to a histogram of ln[Frequency(R_{CO})] versus intervals of R_{CO} values. This histogram can be fitted very well to the following relationship: $\ln(R_{CO}) = -4.077\ R_{CO}^2 + 46.866\ R_{CO} - 130.032$. This can be used to predict the approximate frequency whereby R_{CO} closes to within a plausible covalent bonding distance (e.g., 1.5 Å): approximately 1.2×10^{-30} instances/ns, or a rate of about once every 2.7×10^{13} years. This highly unrealistic finding suggests that Ser 200 deprotonation must not be a precursor to the Ser(O) nucleophilic attack on the ester (or OP) center: an anionic Ser(O) likely experiences too much electrostatic repulsion from the ester (or OP) oxygens to permit nucleophilic attach on the ester (OP) center. A neutral Ser 200 gives a much more plausible result. In this case the logarithmic frequency obeys two very distinct and separate curves of which the one on the right can be interpreted as a lipophilically bound conformer attached primarily to Trp 84, and the other a structure characterized by both lipophilic Trp 84 and polar Ser 200 + His 440 binding. The latter curve permits much closer interaction between the ligand's carbonyl carbon electrophile and the Ser(O) nucleophile, with a logarithmic frequency described by $\ln(R_{CO}) = -3.445\ R_{CO}^2 - 0.334\ R_{CO} + 3.955$. By this relationship, the same 1.5 Å separation is predicted to occur at a rate of 0.1 / ns. Comparing this rate with AChE's known overall ACh processing rate of $\sim10^5$ molecules per second (i.e., 0.001/ns), and recalling the rapidity whereby periferally bound molecules can enter into the gorge (e.g., Fig. 10), it is our assessment that intragorge diffusion is not a rate determining step in the ACh/AChE hydrolysis reaction. Our simulations of OP compounds indicate that they exhibit diffusion behavior that is similar to that of ACh. We find that sarin, for example, exhibits the same sort of bimodal logarithmic frequency plot as ACh. Interestingly, although it spends a significantly greater amount of time in the a bindable conformation at a rate of approximately once every 155 μs – a value that is much greater than that of ACh, but is still less than the total time required for most OP agents to phosphorylate the AChE enzyme (in the ms – minute time frame for ligand concentrations equivalent to fatal doses).

Receptor vibrations that enhance ligand transport behavior have been observed in prior simulations of the AChE receptor. Assuming that the principle function of such sympathetic vibrations is to eliminate log-jam scenarios that would otherwise prevent the ligand from its appropriate intra-receptor transport, we have sought to characterize such phenomena through analysis of rapid jumps in the root mean square deviation (RMSD) of ligand atom positions relative to the starting conformer. Ligand RMSD profiles have thus been plotted and analyzed. The most dramatic shift in conformation occurs for VX between the 100 ps and 200 ps points of the simulation. One finds that the VX shift (a net RMSD of 1.77 Å) corresponds largely to a lurch of more than 1.50 Å away from the periferal site residue Phe 331 and closer to the active site Ser 200. Despite the magnitude of this motion, the RMSD between the corresponding conformations of Phe 330 + Phe 331 is actually very comparable (1.74 Å), moving substantially out of the way of VX in its approach to the receptor. While this shift in these two residues is clearly the key feature of any concerted motion in the protein, the rest of the system does also shift appreciably (net RMSD = 1.20 Å), thus supporting the observation of Shen et al.[14] who suggested broad scale rearrangement in AChE during ligand admission to (or expulsion from) the gorge.

Prediction of Adsorption Kinetics, Thermodynamics, and Physical Properties: Much effort has been devoted to painstaking analysis of the role played by the components of the catalytic triad and the surrounding residues (individually and in concert), and their effect on the catalytic power of the acetylcholinesterase system. Recent proton NMR studies[15] have suggested that formation of a short strong hydrogen bond (SSHB) within the catalytic triad is a key factor in the efficiency of both AChE and the related enzyme butyrylcholinesterase (BChE). These studies have demonstrated a pronounced downfield shift (>15ppm) in the 1H NMR signal, as well as hydrogen bond distances <2.65 Angstroms. We have expanded upon our previous efforts to determine the exact factors contributing to this downfield shift upon binding, with surprising results. Table 1 contains proton NMR shift and residue distances obtained from our quantum calculations for binding (proton and aged DEFP) in three separate models of varying size and complexity. The smallest model contains only the active site residue sidechains (ACTside), used in much of the earlier work (ours as well as others') on this system. The medium sized model contains the full active site residues as well as the full oxyanion hole residues (ACT + OX). The final, largest model expands upon the medium model with the addition of the full neighboring residue Glu199, which has been postulated to play a variety of roles in this system. A close analysis of the distances within the active site (the

Glu327 – His 440 hydrogen bond distance) brings to light very interesting details of this reaction. The experimental data suggests a FURTHER downfield shift in the proton NMR upon binding, specifically from 14.4 ppm for bare acetylcholinesterase to 15.5 and 16.6 for paraoxon (an analogue of DEFP). This coincides with an actual contraction of the hydrogen bonds across the active site residues. The exact numerical values obtained from these models do not invite exact comparison with experimental data, as NMR data is notoriously difficult to obtain to quantitative accuracy. However, the values obtained are all within reasonable accuracy for the method and basis set size used, and shows extremely meaningful trends. To whit, the only model which displays tightening of the active site and a correct downfield shift of the GluH signal relative to the bare system is the largest model containing the Glu199, which in this run has formed a CHO hydrogen bond to the histidine ring (see Figure 2). This conclusively demonstrates the importance of this residue in the binding process, as postulated experimentally.

Table 1.

System	Substrate	Glu327-His440 distance	GluH shift	HisH shift
ACTside	x	2.614	18.972	8.039
ACTside	H	2.712	14.453	11.207
ACT+OX	x	2.584	19.717	12.722
ACT+OX	Aged DEFP	2.651	16.938	14.391
ACT+OX	H	2.693	14.952	11.095
ACT+OX+GLU199	x	2.623	18.854	13.022
ACT+OX+GLU199	Aged DEFP	2.549	21.857	15.601

References

1. Golomb B.A., "A review of the scientific literature as it pertains to Gulf War illnesses." *RAND Report to the Special Assistant to the Deputy Secretary of Defense for Gulf War Illnesses*, Volume 2: Pyridostigmine Bromide, 1999; MR1018/2-OSD: available online at http://www.rand.org/publications/MR/MR1018.2/

2. Zhou, H-X, S.T. Wlodek, and J.A. McCammon, "Conformation gating as a mechanism for enzyme specificity." *Proc .Nat. Acad. Sci. USA*, 95, 1998, pp. 9280–9283.

3. Kryger, G., M. Harel, K. Giles, L. Toker, B. Velan, A., Lazar, C. Kronman, D. Barak, N. Ariel, A. Shafferman, I. Silman, and J.L. Sussman, "Structure of Recombinant Native and E202Q Mutant Human Acetylcholinesterase Complexed with the Snake-Venom Toxin Fasciculin-II." *Acta Crystallogr.*, Sect. D 56, 2000, pp. 1385–1394.

4. Kryger, G., I. Silman, and J.L. Sussman, "Structure of Acetylcholinesterase Complexed with E2020 (Aricept): Implications for the Design of New Anti-Alzheimers Drugs." *Structure*, 7, 1999, pp. 297–307.

5. *Sybyl/Unity 6.9.*, Nov 2002, Tripos, Inc.

6. *Molecular Operating Environment (MOE) 2002.03*, Chemical Computing Group Inc., Mar 2002.

7. Palin, R., J.K. Clark, P. Cowley, A.W. Muir, E. Pow, A.B. Prosser, R. Taylor, and M-Q. Zhang, "Novel Piperidinium and Pyridinium Agents as Water-Soluble Acetylcholinesterase Inhibitors for the Reversal of Neutomuscular Blockade." *Bioorg. Med. Chem. Lett.*, 12, 2002, pp. 2569–2572.

8. Villalobos, A., J.F. Blake, C.K. Biggers, T.W. Butler, D.S. Chapin, Y.L. Chen, J.L. Ives, S.B. Jones, D.R. Liston, A.A. Nagel, D.M. Nason, J.A. Nielsen, I.A. Shalaby, and W.F. White, "Novel Benzisoxazole Derivatives as Potent and Selective Inhibitors of Acetylcholinesterase." *J. Med. Chem.*, 37, 1994, pp. 2721–2734.

9. Clark, J.K, P. Cowley, A.W. Muir, R. Palin, E. Pow, A.B. Prosser, R. Taylor, and M.-Q. Zhang, "Quaternary Salts of E2020 Analogues as Acetylchoinesterase Inhibitors for the Reversal of Neuromuscular Block." *Bioorg. Med. Chem. Lett.*, 12, 2002, pp. 2565–2568.

10. Jones, G., P. Willett, R. Glen, A.R. Leach, and R. Taylor, "Development and Validation of a Genetic Algorithm for Flexible Docking." *J. Mol. Biol.*, 267, 1997, pp. 727–748.

11. *SIMCA-P*, July 2001, Umereics AB.

12. Case, D.A., D.A. Pearlman, J.W. Caldwell, T.E. Cheatam, III, J. Wang, W.S. Ross, C.L. Simmerling, T.A. Darden, K.M. Merz, R.V. Stanton, A.L. Cheng, J.J. Vinvent, M. Crowley, J. Tsui, H. Gohlke, R.J. Radmer, Y. Duan, J. Pitera, I. Massova, G.L. Seibel, U.C. Singh, P.K. Weiner, and P.A. Kollman, "AMBER 6.", University of California, San Francisco, CA.

13. *Gaussian 03, Revision B05*, M.J. Frisch, G.W. Trucks, H.B. Schlegel, G.E. Scuseria, M.A. ; Robb, J.R. Cheeseman, J.A. Montgomery, Jr.,T. Vreven, K.N. Kudin,J.C. Burant, J.M. Millam, S.S. Iyengar, J. Tomasi,V. Barone, B. Mennucci, M. Cossi, G. Scalmani, N. Rega, G.A. Petersson, H. Nakatsuji, M. Hada, M. Ehara, K. Toyota, R. Fukuda, J. Hasegawa, M. Ishida, T. Nakajima, Y. Honda, O. Kitao, H. Nakai, M. Klene, X. Li, J.E. Knox, H.P. Hratchian, J.B. Cross, C. Adamo, J. Jaramillo, R. Gomperts, R.E. Stratmann, O. Yazyev, A.J. Austin, R. Cammi, C. Pomelli, J.W. Ochterski, P.Y. Ayala, K. Morokuma, G.A. Voth, P. Salvador, J.J. Dannenberg, V.G. Zakrzewski, S. Dapprich, A.D. Daniels, M.C. Strain, O. Farkas, D.K. Malick, A.D. Rabuck, K. Raghavachari, J.B.; Foresman, J.V. Ortiz, Q. Cui, A.G. Baboul, S. Clifford, J. Cioslowski,B.B. Stefanov, G.; Liu, A. Liashenko, P. Piskorz, I. Komaromi, R.L. Martin, D.J. Fox, T. Keith, M.A. Al-Laham, C.Y. Peng, A.; Nanayakkara, M. Challacombe, M.; P.M.W. Gill, B. Johnson, W. Chen, M.W. Wong, C. Gonzalez, and J.A. Pople, Gaussian, Inc., Pittsburgh, PA, 2003.

14. Shen T.Y., K.H. Tai, R.H. Henchman, and A.J. McCammon, "Molecular dynamics of acetylcholinesterase." *Accts. Chem. Res.*, 2002; 35, 2002, pp. 332–340.

15. Massiah, M.A., C. Viragh, P.M. Reddy, I.M. Kovach, J. Johnson, T.L. Rosenberry, and A.S. Mildvan, "Short, Strong Hydrogen Bonds at the Active Site of Human Acetylcholinesterase: Proton NMR Studies.", *Biochemistry*, 40, 2001, pp.5682–5690 and references therein.

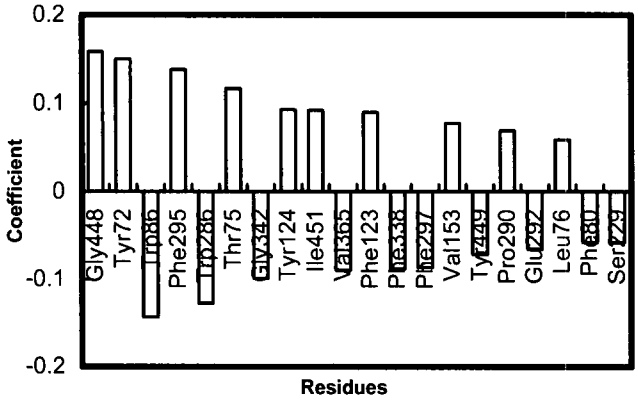

a) Residues importance in VDW interactions

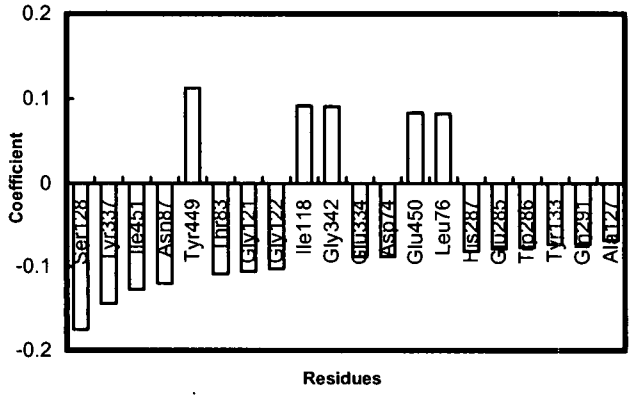

b) Residues importance in electrostatic interactions

Figure 1. a) Coefficients of the 20 most important residues for electrostatic interactions. b) Coefficients of the 20 most important residues for VDW interactions.

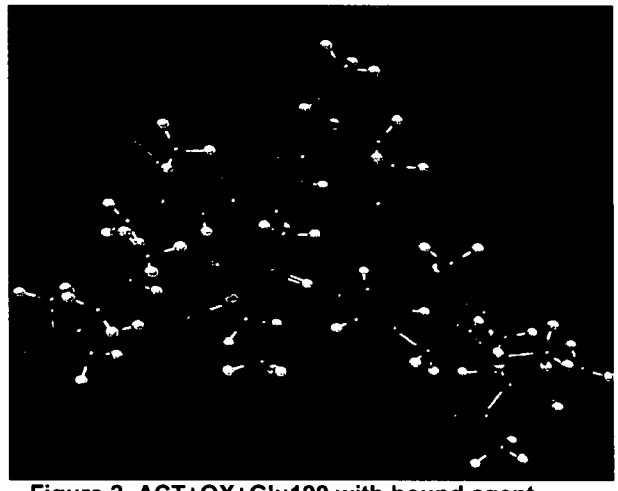

Figure 2. ACT+OX+Glu199 with bound agent stimulant, demonstrating CHO hydrogen bonding of Glu199 to HIS440